



# The structural integrity of the membrane-embedded bacterial division complex FtsQBL studied with molecular dynamics simulations



Yu Wai Chen <sup>\*</sup>, Wai-Po Kong, Kwok-Yin Wong <sup>\*</sup>

State Key Laboratory of Chemical Biology and Drug Discovery, Department of Applied Biology and Chemical Technology, The Hong Kong Polytechnic University, Hung Hom, Hong Kong, China

## ARTICLE INFO

### Article history:

Received 27 January 2023

Received in revised form 30 March 2023

Accepted 31 March 2023

Available online 3 April 2023

### Keywords:

AlphaFold 2

ColabFold

Gromacs

CHARMM-GUI membrane builder

CHARMM36 force field

Transmembrane proteins

Cell division

Divisome

FtsQ

FtsB

FtsL

PBP1b

Protein-protein interaction

## ABSTRACT

The FtsQBL is an essential molecular complex sitting midway through bacterial divisome assembly. To visualize and understand its structure, and the consequences of its membrane anchorage, we produced a model of the *E. coli* complex using the deep-learning prediction utility, AlphaFold 2. The heterotrimeric model was inserted into a 3-lipid model membrane and subjected to a 500-ns atomistic molecular dynamics simulation. The model is superb in quality and captures most experimentally derived structural features, at both the secondary structure and the side-chain levels. The model consists of a uniquely interlocking module contributed by the C-terminal regions of all three proteins. The functionally important constriction control domain residues of FtsB and FtsL are located at a fixed vertical position of ~43–49 Å from the membrane surface. While the periplasmic domains of all three proteins are well-defined and rigid, the single transmembrane helices of each are flexible and their collective twisting and bending contribute to most structural variations, according to principal component analysis. Considering FtsQ only, the protein is more flexible in its free state relative to its complexed state—with the biggest structural changes located at the elbow between the transmembrane helix and the  $\alpha$ -domain. The disordered N-terminal domains of FtsQ and FtsL associate with the cytoplasmic surface of the inner membrane instead of freely venturing into the solvent. Contact network analysis highlighted the formation of the interlocking trimeric module in FtsQBL as playing a central role in mediating the overall structure of the complex.

© 2023 The Authors. Published by Elsevier B.V. on behalf of Research Network of Computational and Structural Biotechnology. This is an open access article under the CC BY-NC-ND license (<http://creativecommons.org/licenses/by-nc-nd/4.0/>).

## 1. Introduction

During bacterial division, the cell wall undergoes hydrolysis and peptidoglycan synthesis which need to be orchestrated precisely. The large and dynamic molecular machinery called the ‘divisome’, a protein complex involving more than 30 components, is responsible for the execution of these tightly-regulated events [1,2]. Interruption or dysfunction in this remodelling process can lead to cell death—a typical example is the inhibition of D,D-transpeptidase by  $\beta$ -lactams, the most commonly used antibiotics [3]. Divisomal proteins are therefore potential targets in the search for new antibiotics [4].

**Abbreviations:** PE, phosphatidylethanolamine; PG, phosphatidylglycerol; CL, cardiolipin; POPE, 1-palmitoyl-2-oleoyl-sn-glycero-3-phosphoethanolamine; POPG, 1-palmitoyl-2-oleoyl-sn-glycero-3-phosphoglycerol; TYCL2, tetrapalmitoleoyl cardiolipin (–2 charged) (16:1<sup>cis9,10</sup> tails)

<sup>\*</sup> Corresponding authors.

E-mail addresses: [yu-wai.chen@polyu.edu.hk](mailto:yu-wai.chen@polyu.edu.hk) (Y.W. Chen), [kwok-yin.wong@polyu.edu.hk](mailto:kwok-yin.wong@polyu.edu.hk) (K.-Y. Wong).

The Gram-negative bacteria *Escherichia coli* is often taken as the model organism in the study of cell division [5,6]. Although the proteins involved have been identified, the molecular details of how they assemble into the divisome and trigger septum synthesis remain poorly understood [6,7]. Over the years, it has been established that this is a hierarchical signalling process [8] occurring at the inner membrane. The first step is the assembly of a ‘Z ring’ by polymerization of the tubulin homologue, FtsZ, at the division site [9]. The Z ring is tethered to the inner membrane by FtsA [10] and ZipA [11]. FtsEX, an ATP-binding transporter-like complex, then migrates to the Z-ring [12]. During this step, several essential division proteins are recruited sequentially: FtsK [13], the FtsQ:FtsB:FtsL (FtsQBL; colon denotes non-covalent protein-protein association) complex [14], FtsW [15], FtsI (aka PBP3) [16] and FtsN [17].

*E. coli* FtsQ is a bitopic membrane protein of 276 residues, including a short cytoplasmic N-terminal domain (NTD), a single-helix transmembrane (TM) segment and a large periplasmic domain [18]. The structure of the periplasmic domains of FtsQ (FtsQ<sub>p</sub>) has been revealed by X-ray crystallography to be consisting of the  $\alpha$ - and  $\beta$ -

<https://doi.org/10.1016/j.csbj.2023.03.052>

2001-0370/© 2023 The Authors. Published by Elsevier B.V. on behalf of Research Network of Computational and Structural Biotechnology. This is an open access article under the CC BY-NC-ND license (<http://creativecommons.org/licenses/by-nc-nd/4.0/>).

domains [18]. The  $\alpha$ -domain together with the transmembrane domain interact with the upstream FtsK [19].

FtsB and FtsL are small bitopic proteins (of 103 and 121 residues, respectively) with relatively large periplasmic domains that are predicted to form  $\alpha$ -helical structures [20,21]. The crystal structure of a fragment of FtsB comprising 30 membrane-proximal periplasmic amino acids was solved as a fusion with Gp7 [22]. This structure shows that the coiled-coil domain of FtsB promotes dimerization, and it is conceivable that FtsB and FtsL interact similarly. The soluble periplasmic complex of FtsQ, FtsB and FtsL (FtsQ<sub>p</sub>B<sub>p</sub>L<sub>p</sub>) can be readily prepared in vitro and was studied by site-specific photo-cross-linking [23], surface plasmon resonance [24], native mass spectrometry [24] and molecular modelling [25]. Evidently, FtsB and FtsL interact with both the  $\alpha$ - and the  $\beta$ -domains of FtsQ. Native mass spectrometry on FtsQ complexed with a constrained dimer of FtsB:FtsL revealed a strong and abundant 1:1:1 trimeric arrangement of FtsQ<sub>p</sub>B<sub>p</sub>L<sub>p</sub> [24], although molecular modelling indicated that both 1:1:1 trimeric and 2:2:2 hexameric complexes are plausible [25].

The FtsQBL complex lies midway of divisive assembly and is essential for cell division [26]. Studies on variants of FtsA, FtsQ, FtsB, FtsL and FtsN suggested a dynamic model as follows [27]. FtsA may exist in one of two conformations that is related to its polymeric status. In the 'on' state, it interacts with FtsN and the FtsQBL complex in the cytoplasm, thus bringing them together. FtsQBL is activated by FtsN so that it interacts with FtsW and FtsI to trigger septal peptidoglycan synthesis. Residues 55–59 on FtsB and 88–94 on FtsL are coined the 'constriction control domains' (CCDs)—the mutations of which lead to the independence from FtsN for activation [27]. Bacteria with FtsL that has its cytoplasmic domain removed ( $\Delta$ 1–30) are unable to recruit the downstream FtsWI complex, but could be rescued by activation mutations in the FtsL CCD (G92D and E88K) [28]. On the other hand, FtsL AWI (activation of FtsWI) residues R82, N83, L84, L86, E87, and A90, when mutated, became dominant negative and led to an FtsQBL complex that cannot be activated by FtsN [28].

There have been several experimental attempts to derive structural information about the FtsQBL complex, including our use of hydrogen/deuterium exchange mass spectrometry (HDX-MS) to study the detergent-solubilized full-length complex of *E. coli* [29]. Until very recently, most of these studies were confined to the periplasmic soluble domains and their artificial fusion derivatives. At the time of writing, a preprint has appeared reporting the cryo-electron microscope structure of the FtsQBLWI complex of *Pseudomonas aeruginosa* [30]. The *P. aeruginosa* and *E. coli* proteins share a homology of 55–58% (FtsQ: 27% identity, 57% similarity; FtsB: 32% identity, 58% similarity; and FtsL: 30% identity, 55% similarity), according to the EMBL-EBI [31], and thus the global structures are expected to be similar. Here we report a computational study using a structural model of the full-length complex generated by the artificial intelligence prediction utility, AlphaFold 2. The trimeric complex model was inserted into a 3-lipid model membrane and subjected to a 500-ns atomistic molecular dynamics (MD) simulation. When the trajectory of the FtsQBL complex and that of free FtsQ were compared, the structural implications of the formation of the complex began to emerge.

## 2. Results

### 2.1. AlphaFold 2 model agrees with structural data

The AlphaFold 2-predicted FtsQBL model captures all important features from previous structural studies. The two periplasmic domains of FtsQ were predicted accurately (root-mean-square deviation, RMSD, of all C $\alpha$  atoms with PDB ID 2VH1 = 1.7 Å, 203 residues).

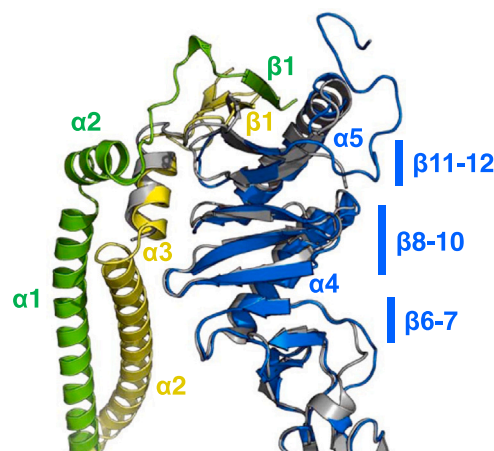


**Fig. 1.** FtsQBL model agrees with the crystal structure. The crystal structure of FtsQ in complex with FtsB (PDB ID 6H9N) is shown in grey cartoons. The AlphaFold 2-predicted model is superimposed and coloured with FtsQ in blue, FtsB in yellow and FtsL in green.

Remarkably, even the relative spatial relationships of the three transmembrane helices are physically compatible so that the helices could be readily placed into a membrane layer (Fig. S1c). The interaction of FtsQ with FtsB was modelled correctly (Fig. 1; RMSD of all C $\alpha$  atoms with PDB ID 6H9N = 1.7 Å, 227 residues). FtsB and FtsL form a long coiled-coil extending from the paired transmembrane helices, with FtsB having a break at the transmembrane-periplasmic interface. FtsQ transmembrane domain does not interact with those of FtsB and FtsL [32]. In fact, there is little or no direct interaction between FtsQ and FtsL [30,33]. These excellent agreements with experimental evidence at the backbone and secondary structure level encouraged us to proceed with the MD studies.

### 2.2. Predicted trimeric interface

We examined more closely, at the side-chain level, the details of how FtsQ and FtsB interact. Here, the most representative model from the MD simulation was compared to the crystal structure of the FtsQ:FtsB complex [34]. FtsQ Y248, a conserved residue at the FtsQ-FtsB interface, is a crucial residue for binding FtsB. Its conformation changes significantly on complexation [33]. The central role of Y248 is reflected in the most representative model. FtsQ Y248 is surrounded by the FtsB kinked loop and stabilized by an intramolecular salt-bridge and hydrogen-bond network involving FtsB residues E68, R72, R79, and E82 [33,34]. These charged residues of FtsB form electrostatic interactions with FtsQ D245 and R247 [33]. FtsQ R196 forms a salt bridge with FtsB E69 [34]. All these interactions were maintained in the most representative model of the MD simulation (Fig. 2).

FtsB F84 is in contact with FtsQ Y248, whereas FtsB Y85 packs on a cluster of hydrophobic residues of FtsQ: L226, L230, V254, W256 [34]. FtsB L87 also packs on FtsQ L226 and R222. These interactions were preserved in the most representative model.

In the crystal structure, FtsB strand  $\beta$ 1 consists of 4 residues (83–86) and runs antiparallel to the last FtsQ strand,  $\beta$ 12, expanding the FtsQ  $\beta$ -sheet by one strand. In the AlphaFold 2 model, FtsB strand  $\beta$ 1 expands to six residues (83–88) (Fig. 1). Up to here, the AlphaFold 2-model captures the known structural features faithfully which were maintained in the simulation trajectory (Fig. 2).

AlphaFold 2 predicted that FtsQ, FtsB and FtsL form a 1:1:1 complex (Supplementary information). This model uniquely proposes that the FtsL C-terminal region folds into two secondary structural elements to facilitate the formation of the trimer. First, the FtsL C-terminal residues 116–120 form a strand  $\beta$ 1 which runs

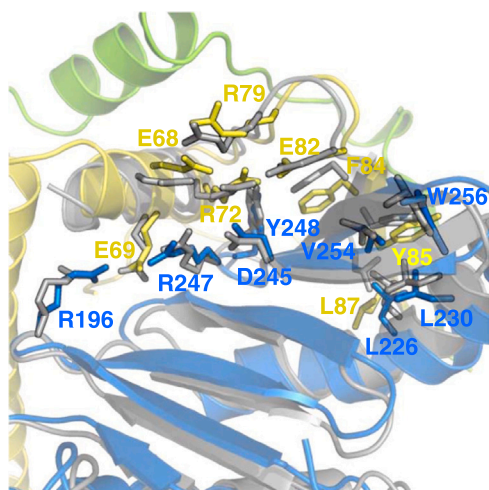


**Fig. 2.** FtsQBL MD model preserved key FtsQ-FtsB interacting residues. The crystal structure of FtsQ in complex with FtsB (PDB ID 6H9N) is shown in grey cartoons. The most representative MD model of FtsQBL is superimposed. The cartoons were coloured with FtsQ in blue, FtsB in yellow and FtsL in green. The side chains of important interacting residues are shown as sticks.

parallel to FtsB  $\beta$ 1 (Fig. 1). As a result, the 12-stranded  $\beta$ -sheet of FtsQ becomes a 14-stranded one in the trimeric complex. This is in excellent agreement with a newly solved structure of FtsQBLWI [30]. At the end of the long helix of FtsL, it breaks to form the  $\alpha$ 2 helix, which packs on FtsB  $\alpha$ 3 with their axes almost perpendicular to each other (Fig. 1). These two FtsL secondary structural elements reinforce the FtsQ-FtsB interface to establish the complete trimeric interface.

### 2.3. The FtsQBL complex is stable

The analysis of atomic displacement of core residues (the best-aligned 70% of all residues has an RMSD of  $C\alpha$  atoms of 2.5 Å) revealed that the complex structure was stably maintained throughout the simulation (Fig. 3a). The remaining 30% subset of residues represents the flexible and variable residues. The RMSF of the  $C\alpha$  atoms of the model is an indication of the extents of movement, i.e. rigidity, of the protein backbone. The RMSF plot shows that the variable regions are at both termini of FtsQ, the C-terminus of FtsB, and the N-terminus of FtsL (Fig. 4a). Namely, these residues, having an RMSF > 8 Å, are FtsQ residues 1–27 and 261–276, FtsB residues 93–103, and FtsL residues 1–34. The transmembrane helices are more variable than the periplasmic domains in general. The

characteristic downward-sloping regions on the RMSF plot (Fig. 4a:  $\alpha$ 0 of FtsQ,  $\alpha$ 1 of FtsB and  $\alpha$ 1 of FtsL) indicate bending of the helices, relative to the most representative model. Thus, the residual RMSF values of the transmembrane regions reflect the effect of helix bending in addition to local flexibility.

### 2.4. The FtsQBL complex is rigid with bendable anchors

The first three principal components (PC1 to PC3) captured 72% of the structural variance (Fig. S2e). PC1 represents 47% of the variance in structural changes, but there are little contributions from the entire periplasmic domain of FtsQ (Fig. S2a). The largest atomic displacements are observed at the N-terminal regions of both FtsB and FtsL (Fig. 5, S2a), including both transmembrane helices. Although the residues form regular helical secondary structures, there are rigid-body displacements relative to the whole complex. These characteristically manifest as downward sloping regions in PC1: FtsB ( $\alpha$ 1,  $\alpha$ 2 and  $\alpha$ 3) and FtsL ( $\alpha$ 1 and  $\alpha$ 2) (Fig. S2a). The cytoplasmic domain of FtsL is also highly variable. Thus, the complex has a well-defined structural core sitting on three anchors embedded in the membrane, with the two legs of FtsB and FtsL undergoing twisting and bending movements.

### 2.5. FtsQ in its free and bound states

Next, we compared the overall structural variations of FtsQ in its free and bound states (Table 1 and Fig. 3). The free FtsQ has a 70%-core RMSD of 2.0 Å and an overall RMSD of 6.6 Å (Fig. 3c). The complexed FtsQ has a 70%-core RMSD of 1.4 Å and an overall RMSD of 5.3 Å (Fig. 3b). As expected, the overall structural variation of FtsQ is substantially reduced in the complex. The individual FtsQ component among the complex is better defined than the complex as a whole, which has a 70%-core RMSD of 2.5 Å.

The overall  $C\alpha$  RMSF of the ordered region (residues 56–257) of the FtsQ periplasmic domain of the free protein and that in the FtsQBL complex were  $2.0 \pm 0.06$  Å (standard deviation, SD = 0.8 Å) and  $1.5 \pm 0.04$  Å (SD = 0.6 Å), respectively (Fig. 4b). The FtsQ periplasmic domain is thus significantly more rigid when the complex forms. The RMSF of the FtsQ  $\beta$ -domain (residues 160–257) and that of the  $\beta$ 3 to  $\beta$ 5 hinge region (residues 124–139) decreased similarly by  $\sim 0.5$  Å, in the FtsQBL state compared to those in the free state. These increases in rigidity on complexation were not as significant as our previous study at the minute scale [29]. Noticeably, two regions in FtsQ have RMSF reduced by > 1 Å on complexation, namely, residues 79–92 (loop between  $\alpha$ 1 and  $\alpha$ 2) and 226–241 (C-terminal half of  $\alpha$ 5 and its trailing loop). The loop between  $\alpha$ 1 and  $\alpha$ 2 is close

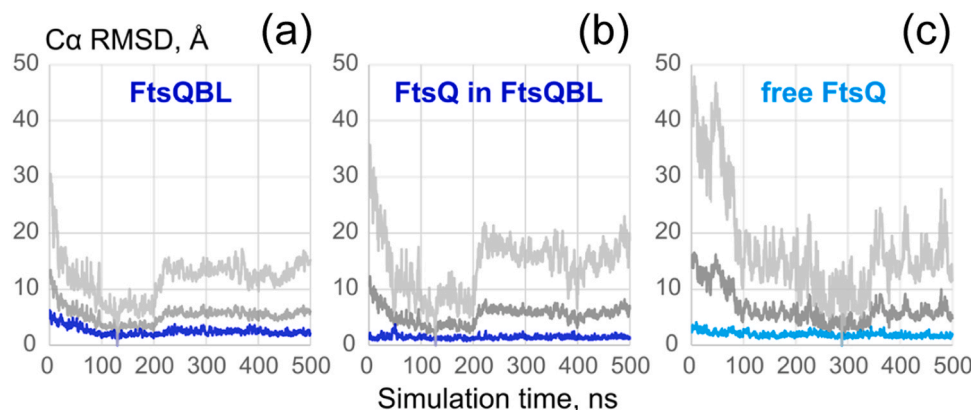


**Fig. 3.** Structural stability of FtsQ and FtsQBL in the MD simulations. The RMSD of  $C\alpha$  atoms was analyzed such that 70% of the least mobile atoms constituted the core. (a) The FtsQBL complex as a whole (total of 500 residues), with its core RMSD in blue. (b) The FtsQ component (276 residues) within the FtsQBL complex with its core RMSD, also in blue. (c) The free FtsQ protein with its core RMSD in cyan. In all three plots, the overall curves are in dark grey (middle curves) and the remaining 30% RMSD curves (the RMSD of the non-core residues) in light grey (top curves).



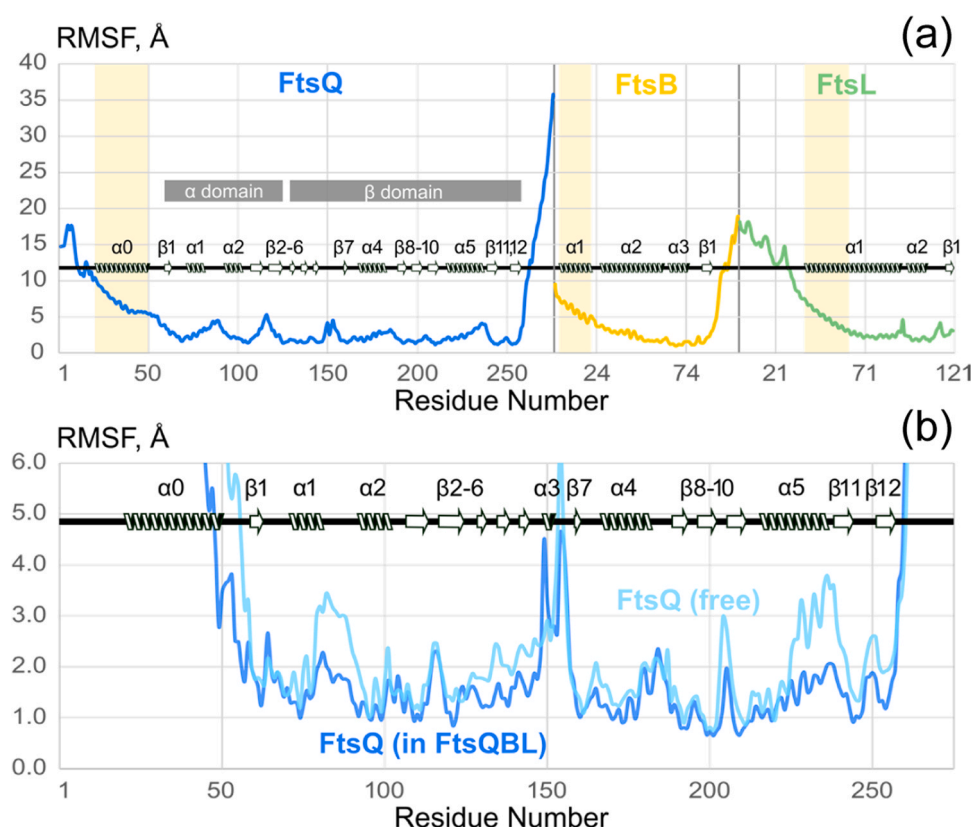


**Fig. 4.** Structural fluctuations of FtsQ and FtsQBL in the MD simulations compared. The RMSF of C $\alpha$  atoms was analyzed with MDlovoFit with 70% of the least mobile atoms constituting the protein or complex core. (a) The FtsQBL complex as a whole (total of 500 residues), with its respective components coloured (FtsQ in blue, FtsB in yellow and FtsL in green). The secondary structures observed in the simulation were shown. The transmembrane regions were shaded. (b) The RMSF of the FtsQ component within the FtsQBL complex (in blue) compared with that of the free FtsQ protein (in cyan).

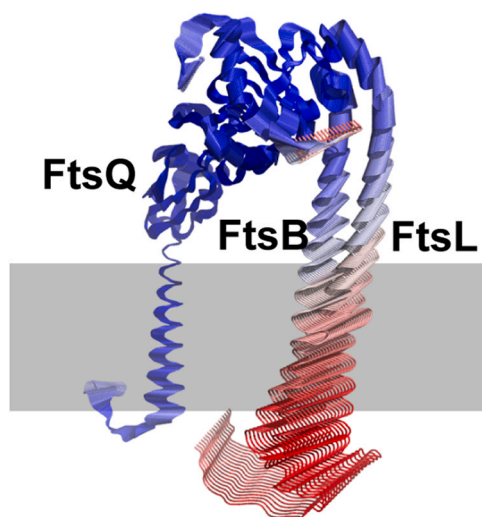


**Fig. 5.** The first principal component (PC1) of the FtsQBL complex in MD simulation. The protein complex was shown as a C $\alpha$  trace, with colours representing relative atomic displacements in the PC1 from blue (small) to white (medium) to red (large). The membrane is represented by the grey shaded region.

to the hinge (residues 49–59) connecting the transmembrane helix and the whole periplasmic domain. On forming the complex, the whole periplasmic domain of FtsQ is locked into one configuration by anchoring with FtsB and FtsL, and this hinge is no longer flexible. However, this dynamic change was not detected experimentally [29]. The flexibility of FtsQ residues 226–241 is lost on complexation because they are in the vicinity of the three strands (FtsQ  $\beta$ 12, FtsB

**Table 1**  
RMSD of the FtsQBL complex and FtsQ in MD simulation.

	FtsQBL complex	FtsQ in FtsQBL	FtsQ (free)
RMSD (Overall), Å	5.34 $\pm$ 0.05	5.32 $\pm$ 0.05	6.55 $\pm$ 0.09
RMSD (Core, 70%), Å	2.51 $\pm$ 0.02	1.45 $\pm$ 0.01	1.96 $\pm$ 0.02
RMSD (Other, 30%), Å	11.94 $\pm$ 0.12	14.33 $\pm$ 0.16	17.21 $\pm$ 0.29

In each case, the most representative structure from cluster analysis was used as the reference.

$\beta$ 1, and FtsL  $\beta$ 1) at the trimeric interface. This is in good agreement with HDX-MS results [29].

We next attempted to locate the major structural changes of FtsQ on complexation. A difference distance matrix was calculated between the complexed and the free states. Only six significant distance changes were detected, and they all involved the residues at the hinge region between the transmembrane helix and the  $\alpha$ -domain (residues 49–53). The pairs of residues and their respective differences in C $\alpha$ -distance (complexed state minus free state) are: E50-T89 (–7.3 Å), E50-M88 (–5.9 Å), M49-M88 (–5.7 Å), Q53-M88 (4.9 Å), E50-Q53 (3.4 Å), and M49-A52 (3.3 Å). These changes reflect the different hinge configurations between the two states. The top three negative changes reflect the loop connecting  $\alpha$ 1 and  $\alpha$ 2 (residues M88 and T89) moves closer to the C-terminal end of the transmembrane helix (residues M49 and E50) to form an ‘elbow’ (Fig. 6). In the free FtsQ, the C-terminal end of the transmembrane helix forms one more turn.

## 2.6. FtsQ transmembrane helix is tilted

In the FtsQBL complex, all the transmembrane helices of FtsQ, FtsB and FtsL are embedded in the membrane with an angle to the

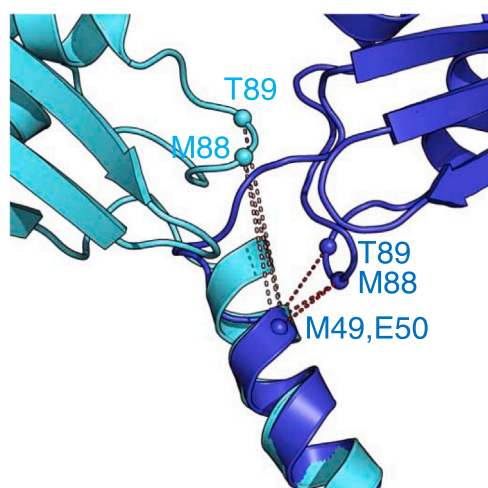


**Fig. 6.** The structural differences of FtsQ between its free and complexed states. The free (cyan) and complexed (blue) models were aligned on the transmembrane helices. C $\alpha$  atoms of interest are shown as spheres. The distances were shown in pink (free state) and red (complexed state) broken lines.

normal of the membrane surfaces. The transmembrane helix ( $\alpha 0$ ) of FtsQ in the FtsQBL complex has an average tilt angle of  $23.3^\circ$  (SD =  $4.7^\circ$ ), whereas that of the free FtsQ is very similar, of  $23.7^\circ$  (SD =  $6.7^\circ$ ) (Fig. S3), suggesting that the transmembrane helix tilt is not a structural consequence imposed by the formation of the complex. It is interesting to note that at the beginning of the simulation, the free FtsQ transmembrane helix has a small tilt angle, of  $5.2^\circ$ , which progressively increased to  $\sim 20^\circ$  within 50 ns (Fig. S3, cyan curve). This was because the free FtsQ model was inserted vertically into the membrane roughly along the axis of the transmembrane helix. Contrasting to this, the FtsQBL complex predicted by AlphaFold 2 has the three transmembrane helices of FtsQ, FtsB and FtsL arranged in a manner that dictates their insertion into the model membrane, with the FtsQ transmembrane helix already at a tilt angle of  $\sim 20^\circ$  (Figs. S1c, S3).

## 2.7. Constriction control domains are fixed vertically

It was speculated that one of the major structural consequences of the FtsQBL complex is to keep the FtsB and FtsL CCDs at a fixed vertical position from the membrane surface [29]. The center of geometry of C $\alpha$  atoms of both CCDs were obtained from the simulation. The FtsB CCD was at  $\sim 43$  Å (SD = 2.6 Å) from the membrane surface, whereas that of FtsL was at  $\sim 49$  Å (SD = 2.7 Å). The respective small standard deviation values indicated that these vertical distances were kept relatively constant. This agrees with the notion that the CCD represents a binding module of the FtsQBL complex to downstream divisomal proteins, now known to include FtsI, that requires certain height from the membrane surface [30].

The MD most-representative model supplies atomic details of the CCDs that can be validated with experimental data of the *P. aeruginosa* FtsQBLWI (PaFtsQBLWI) structure [30]. The CCD residues of FtsB and FtsL pack against a positively charged cluster consisting of FtsQ R196 (equivalent to PaFtsQ R214), FtsQ R213 (PaFtsQ R231) and FtsB R70 (PaFtsB R75). The negatively charged CCD residues FtsB E56 and D59 (PaFtsB E61 and E64), and FtsL E88 (PaFtsL Q65) interact with the oppositely charged cluster. These charged interactions agree well with the information extracted from the *P. aeruginosa* structure (Fig. S4). The AWI residue FtsL L84 (PaFtsL L61) contributes hydrophobic interactions to maintaining the FtsBL coiled-coil (Fig. S4). It is conceivable that a charged residue (K/D) replacement produces the dominant negative phenotype because the FtsBL coiled-coil is disturbed, close to the CCDs.

## 2.8. Terminal disordered domains of FtsQ, FtsB and FtsL

At the beginning of the simulation, both N-terminal cytoplasmic regions of FtsQ and FtsL were modelled to be unstructured extended coils surrounded by the solvent. After the little restraint force imposed in the last step of equilibration was removed, within 50 ns, both regions withdrew from the solvent and lied flat on the cytoplasmic surface of the membrane and remained so till the end. The cytoplasmic domain of FtsQ on its own also exhibited this effect. It appeared that these regions prefer to associate with the membrane surface environment rather than with the solvent, presumably due to more favourable hydrophobic and electrostatic interactions. The association with the membrane surface of the N-terminal regions may be essential for interacting with the upstream divisomal proteins [27]. For instance, the cytoplasmic protein FtsA has an amphipathic C-terminal helix that interacts with the cytoplasmic face of the inner membrane [35], thereby tethering the Z ring to the membrane.

The C-terminus of FtsQ, residues 261–276, is disordered in the AlphaFold 2 model (Fig. S1b). Nevertheless, the network analysis of trajectories indicated that this tail became substantially more closely associated with the  $\alpha$ - and  $\beta$ -folded domains when FtsQ complexed with FtsBL (see later). The C-terminal tail of FtsB (residues 92–103) remained unstructured in the simulations.

## 2.9. Correlated displacement of protein regions

The dynamic cross-correlation matrices were calculated for the FtsQBL complex and the free FtsQ trajectories (Fig. 7). The positive off-diagonal slanted regions between FtsB and FtsL reveal the coiled-coil arrangement between them (Fig. 7, labelled 'A'). Positive correlations are showing the interactions of the FtsQ upper  $\beta$ -domain with the FtsB C-terminal region strand (Fig. 7, labelled 'B') and with the FtsL C-terminal strand (Fig. 7, labelled 'C'). Free FtsQ exhibits strong anti-correlations in some regions, the most noticeable one being between the  $\alpha$ -domain and the upper (C-terminal) half of the  $\beta$ -domain (Fig. 7, labelled 'D'). In the complexed FtsQ, this anti-correlation is not so pronounced. If we focus on the  $\beta$ -domain, the complexed FtsQ has generally more intra-domain positive correlations, particularly in the lower half subdomain of  $\beta$  (residues 126–185). This subdomain also has more positive correlations with the  $\alpha$ -domain of FtsQ in the complexed state. Overall, the complexed FtsQ shows more positive cross-correlations, supporting that the protein becomes more rigid when it is bound to FtsB and FtsL.

## 2.10. Contact network analysis of the FtsQBL complex and of free FtsQ

The FtsQBL complex, of 500 nodes and 3168 edges, was clustered into a coarse-grained contact network of 10 communities with 10 edges, at a modularity of 0.65 (Fig. 8a,b; Table 2). This analysis revealed that the whole trimeric complex follows a linear topology, from the cytoplasmic N-terminus of FtsQ to the transmembrane helix, the  $\alpha$ - and  $\beta$ -domains of FtsQ, to the FtsQBL interaction interface, to the long coiled-coil of FtsBL, to the cytoplasmic N-terminus of FtsL (Fig. 8a,b). Most nodes only contact adjacent nodes. FtsB and FtsL interact extensively and behave as a lower coiled-coil and an upper coiled-coil. Community 5 represents the trimeric interacting module and includes residues of FtsQ, FtsB and FtsL which interlock into a single big domain. The consensus contact network of FtsQ consists of 6 communities in common with the first six (1–6) of the FtsQBL network (Fig. 8c). When the network of the trimeric complex is compared with the consensus network of FtsQ, it is obvious that there is a big difference in the number of residues defining this interfacing module of FtsQ (Fig. 8b, c). In the free protein, the residues responsible for interaction make fewer contacts. Some of them partition into the lower  $\beta$  domain, i.e. free FtsQ has a bigger



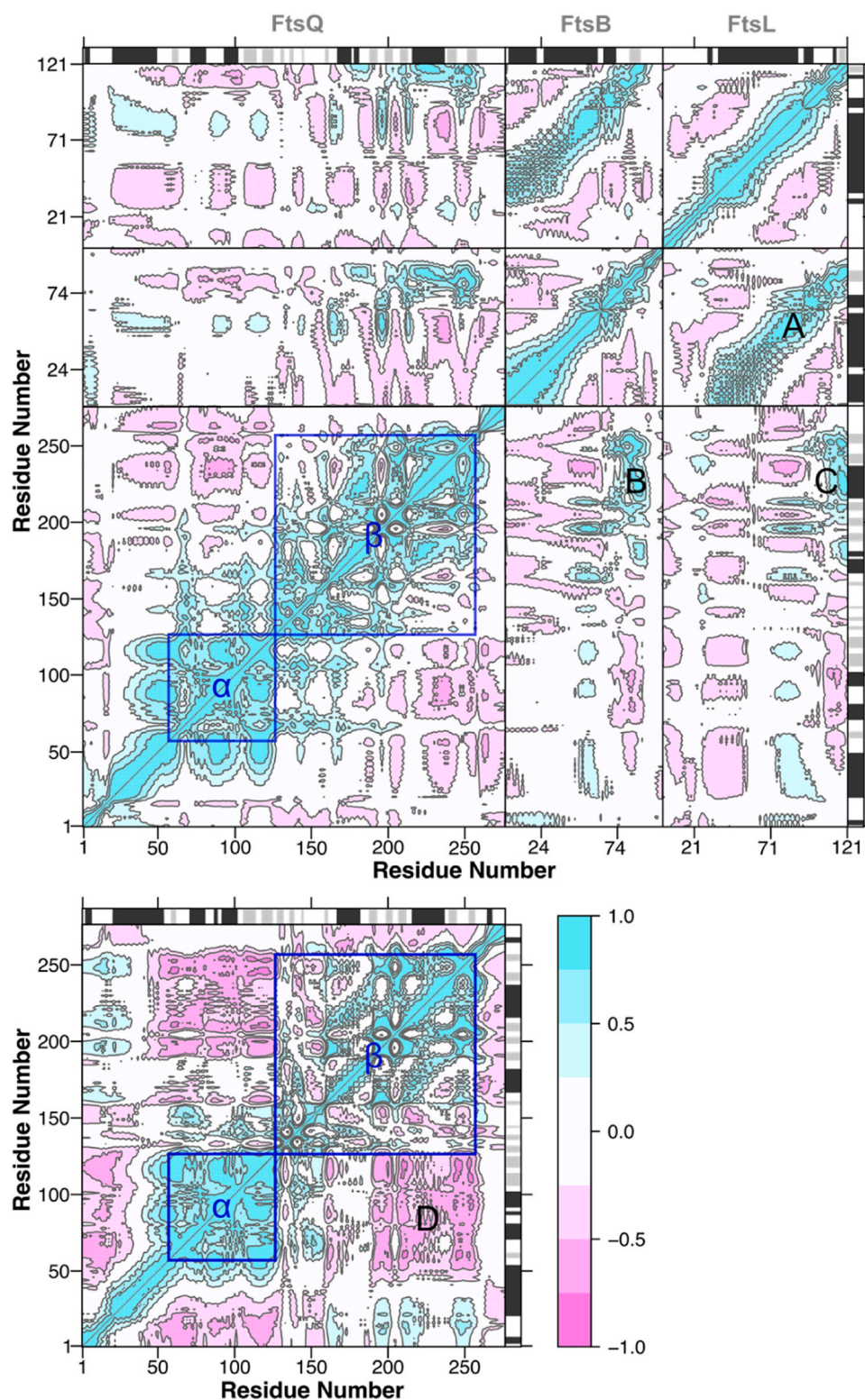


**Fig. 7.** The dynamic cross-correlation matrix of the FtsQBL complex and that of FtsQ. The maps were scaled to be from -1 (anti-correlated, in magenta) to 1 (fully correlated, in cyan). The secondary structures were shown in blocks along the right and the top with helices in black and strands in grey. The blue boxes indicate the  $\alpha$ - and  $\beta$ -domains of FtsQ. The regions labelled A-D were discussed in the text.

community 4 than complexed FtsQ (Fig. 8b, c). The difference network analysis informs the changes when FtsQ forms a complex. The major changes involve its C-terminal tail (community 6). While these residues are without defined structure and flexible in the free

protein, they become closely associated with community 4 (the lower  $\beta$ -domain), and also with the  $\alpha$ - and the upper  $\beta$ -domains (Fig. 8c).

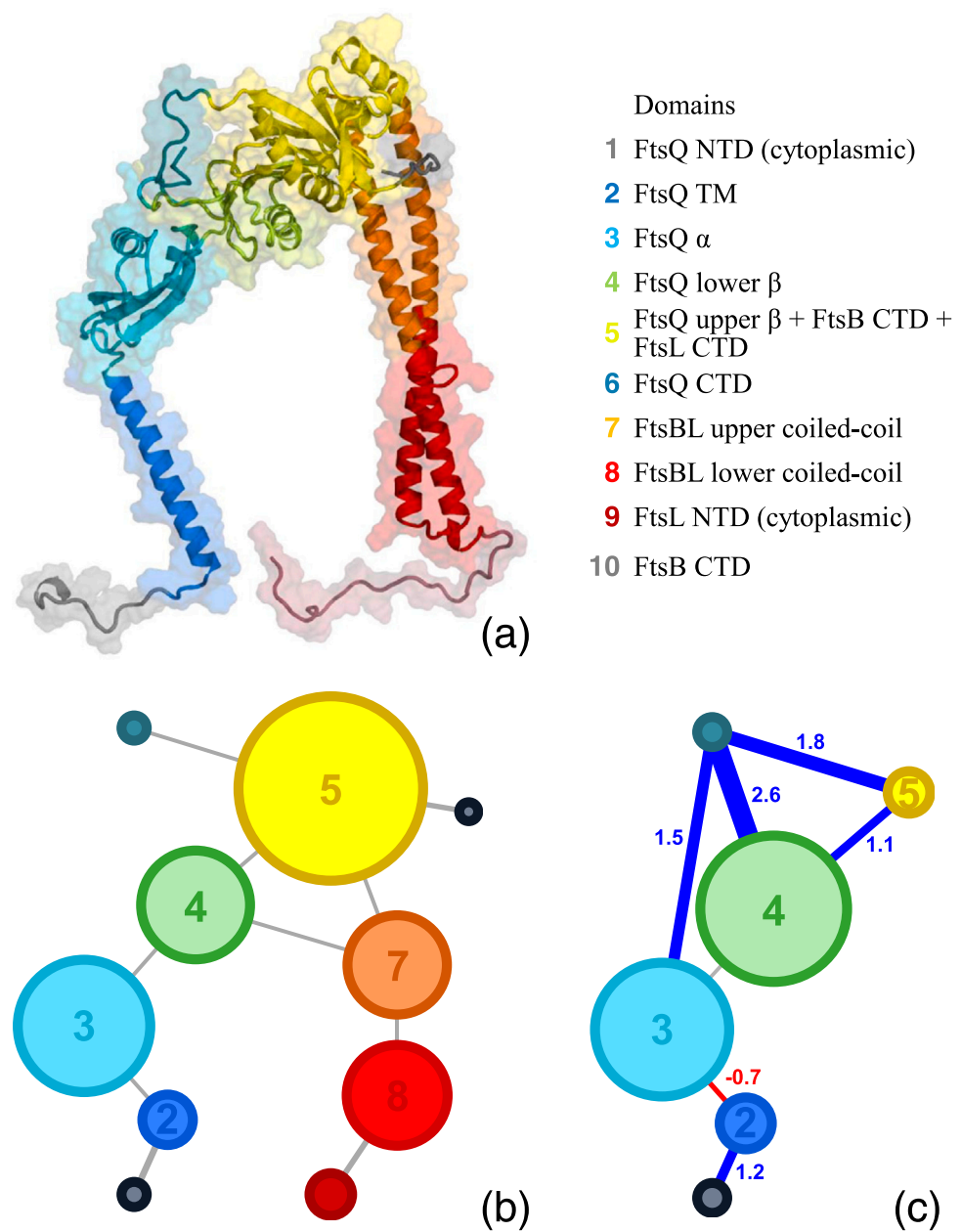


**Fig. 8.** Network analysis of the FtsQBL complex. (a) The molecular model of the FtsQBL complex coloured in the same way as in the contact network for comparison, with the corresponding structural domains. (b) Contact network of the FtsQBL complex with communities shown as circles with radii proportional to their sizes. The relative thickness of edges are proportional to the number of contacts. (c) The difference contact network of FtsQ (FtsQ in FtsQBL minus free FtsQ). Here an increase in number of contacts on complexation is represented by a blue line and a decrease by red.

**Table 2**  
Coarse-grained representations of the FtsQBL complex and that of free FtsQ.

	Domains	Residues (FtsQBL)	Residues (free FtsQ)
1	FtsQ NTD (cytoplasmic)	FtsQ: 1–16	FtsQ: 1–19
2	FtsQ TM	FtsQ: 17–48	FtsQ: 20–52
3	FtsQ $\alpha$	FtsQ: 49–127, 147–151	FtsQ: 53–126, 146–156
4	FtsQ lower $\beta$	FtsQ: 128–146, 152–201	FtsQ: 127–145, 157–220, 244–252
5	FtsQ upper $\beta$ ; FtsB CTD, FtsL CTD	FtsQ: 202–260, FtsB: 63–91, FtsL: 93–121	FtsQ: 221–243, 253–257
6	FtsQ CTD	FtsQ: 261–276	FtsQ: 258–276
7	FtsBL upper coiled-coil	FtsB: 29–62, FtsL: 64–92	—
8	FtsBL lower coiled-coil	FtsB: 1–28, FtsL: 28–63	—
9	FtsL NTD (cytoplasmic)	FtsL: 1–27	—
10	FtsB CTD	FtsB: 92–103	—

For the complex, the analysis was based on its MD trajectory. For FtsQ, the consensus network was built from both the trajectory of the FtsQ component in the FtsQBL complex and that of the free FtsQ. NTD: N-terminal domain; TM: transmembrane domain; CTD: C-terminal domain

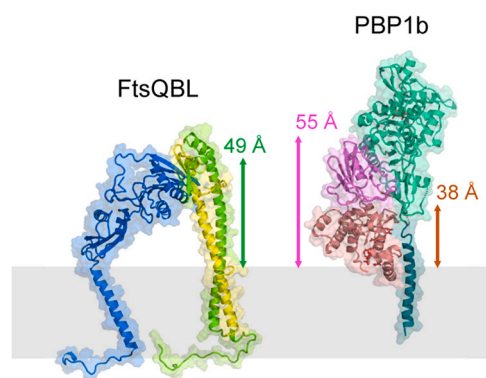


**Fig. 9.** Interaction between FtsQBL and PBP1b. The height of the CCD in FtsL (green) was shown in the FtsQBL complex on the left. The heights to the top of the domains of PBP1b (PDB ID: 5HL9), glycosyltransferase (brown) and UB2H (magenta), are shown on the right. The membrane is represented by the grey shaded box. FtsQ is in blue; FtsB in yellow; PBP1b transmembrane domain in dark green; PBP1b transpeptidase domain in cyan green.

### 3. Discussion

#### 3.1. CCD and PBP1b

The FtsL CCD interacts with the downstream divisomal protein complex FtsWI and/or penicillin-binding proteins (PBP), including PBP1b and PBP3 (aka. FtsI) [28,36]. More precisely, the FtsL CCD suppresses the glycosyltransferase activity in PBP1b [37]. The fixed vertical position of the CCDs observed here may shed some light on the regulatory mechanism of the bifunctional enzyme. From its crystal structure [38], the glycosyltransferase domain of PBP1b lies no taller than 40 Å from the membrane surface. By simple geometric consideration, it is more likely that the FtsQBL complex might act via the FtsBL CCDs on the UB2H domain of PBP1b to effect inhibition (Fig. 9).

#### 3.2. Previous attempts at FtsQBL complex modelling and simulation

The earliest MD simulation of the FtsQ, FtsB and FtsL proteins was an attempt at the complex formed by the corresponding periplasmic domains [25]. This was performed when the norm of MD length was at the 10-ns scale. The compact trimeric (1:1:1) and hexameric (2:2:2) complexes are stable but they are very different from our results as it has FtsQ<sub>p</sub> packing along the whole length of the long FtsB<sub>p</sub>L<sub>p</sub> coiled-coil. Next, there was a study on the FtsBL (2:2) tetrameric coiled-coil embedded in a model membrane [39], using MD runs spanning 200 ns (replica) or 260 ns. The model was based on co-evolutionary analysis and is therefore conceptually related to this study. A later study from the same group used AlphaFold 2-predicted FtsBL (2:2) ‘Y-model’ embedded in a single-component (POPE) membrane model and three MD simulations, each of 400 ns [40]. But the N-terminal domain of FtsL and the C-terminal domains of both FtsB and FtsL were truncated in these two FtsBL studies. Our complex model is not consistent with the two proposed FtsBL (2:2) tetrameric models. In a recent review of the structural aspects of the divisome, the authors used AlphaFold 2-generated models for discussion and they presented an FtsQBL interface very similar to the 14-stranded β-sheet we discussed here (Figure 15 of [41]). Our work reported here initiated as a modelling exercise used in the interpretation of HDX-MS experiments [29]. Another work at the preprint stage reported a POPE-membrane-embedded FtsQBLWI simulation at the 1-μs scale, which also made use of AlphaFold 2 for modelling [42].

The recent trends of studying membrane complexes *in silico* seem to converge to a common workflow: [i] modelling by

AlphaFold 2 implemented in ColabFold, [ii] membrane modelling and protein insertion by CHARMM-GUI Membrane Builder, and [iii] MD simulation at the hundred-ns scale. Our results reported here showed that the methodology is robust and can generate structural knowledge that is in excellent consistency with experimental results.

#### 3.3. Sampling of atomistic membrane-protein simulation

The conformational dynamics of membrane-embedded proteins are often studied at the hundred-nanosecond to microsecond time scale [43–46]. We employed all-atom systems with explicit solvent (totalling ~450,000 and ~500,000 atoms, respectively) so that structural information at the side-chain level can be extracted. To strike a compromise between resolution and sampling, a single trajectory was run for 500 ns for each experiment. The length was comparable with similar studies [43,44,46] but the sampling of the conformational space may not be thorough—this is the limitation of this study. Ideally, multiple independent runs should be performed. For instance, in the porin work, 10 independent 1-μs replicas were run [46]. Alternatively, different initial structures were used [47].

### 4. Materials and methods

#### 4.1. Model of the FtsQBL complex

We employed the ColabFold notebook [48] interface to produce the FtsQBL (1:1:1) trimeric complex model. The *AlphaFold2\_advanced (beta)* notebook, which implemented AlphaFold version 2 [49] in combination with MMseqs2 [48] for multiple sequence alignment and without using templates, was run on the Google Colab service. The only inputs were the three protein sequences (UniProtKB entries: EcFtsQ, P06136; EcFtsB, P0A6S5; EcFtsL, P0AEN4) and the multimer stoichiometry. The top-ranking predicted model was subjected to a refinement step in Modeller version 9.21 [50], using the altMOD plugin [51], to rebuild the N- and C-termini with low pLDDT (predicted score based on the local distance difference test Cα-metric) scores (<70): FtsQ residues 1–21 and 262–276, FtsB residues 1 and 91–103, and FtsL residues 1–36 and 121. This step was necessary because AlphaFold tends to render unreliable regions into helices (see Fig. S1c).

The model of full-length FtsQ was generated in the same way with only the sequence, followed by Modeller refinement of residues 1–23 and 262–276 (pLDDT < 70).

#### 4.2. Model of the *E. coli* inner membrane

The bacterial cell membrane is dynamic and the lipid composition varies with the life cycle to facilitate specific physiological responses [52]. The basic composition is relatively stable: ~75–80% PE, ~20% PG and ~5–10% CL [52–54]. We assembled our inner membrane model referencing the asymmetric model of Bogdanov *et al* (2020). It adopted a ratio of 3:1 on the number of PE in the cytoplasmic leaflet to that in the periplasmic leaflet [55]. The most abundant fatty-acid tails are of: 16:0 (palmitoyl-), 16:1 (palmitoleoyl-), and 18:1 (oleoyl-) [54]. Therefore, we used POPE and POPG (both with 16:0 and 18:1 tails) in place of DOPE (dioleoyl-phosphatidylethanolamine) and DOPG (Dioleoyl-phosphatidylglycerol). For cardiolipin, we used TYCL2 instead of TOCL2 to reflect the abundance of the 16:1<sup>cis9,10</sup> fatty-acid tails [54,55].

The trimeric FtsQBL complex model was manually orientated and then inserted into the asymmetric membrane with the help of the CHARMM-GUI Membrane Builder [56], which generated the topology and parameters with the CHARMM36 force field [57], as well as the MD strategy and running scripts for Gromacs. The Z dimension was set to have a water layer on each face of the membrane of at



**Table 3**The composition of the model *E. coli* inner membrane used in this study.

Membrane Area, Å <sup>2</sup>	Lipids	Fatty acid tails	Periplasmic leaflet	Cytoplasmic leaflet
Initial, 80 × 80	POPE	16:0 / 18:1	25 (25%)	75 (75%)
	POPG	16:0 / 18:1	65 (65%)	15 (15%)
	TYCL2	16:1 × 4	5 (10%)	5 (10%)
Expanded, 150 × 150	POPE	16:0 / 18:1	90 (25%)	285 (75%)
	POPG	16:0 / 18:1	234 (65%)	57 (15%)
	TYCL2	16:1 × 4	18 (10%)	19 (10%)
Final, 150 × 150	POPE	16:0 / 18:1	95 (25%)	285 (75%)
	POPG	16:0 / 18:1	239 (65%)	57 (15%)
	TYCL2	16:1 × 4	19 (10%)	19 (10%)

least 22.5 Å thickness. The length of XY dimensions was based on the number of lipids. Initially, a guessed attempt of building the membrane with an XY = 80 × 80 Å<sup>2</sup> leaflet (top rows of Table 3) resulted in an area that was too small. The system was expanded to XY = 150 × 150 Å<sup>2</sup> while keeping the ratios of lipid components fixed (Table 3, middle rows). The actual number of each lipid used was determined empirically and manually adjusted (Table 3, bottom rows) to satisfy the density requirements of the Membrane Builder, i.e. the upper leaflet can accommodate more lipids. The system included 0.15 M NaCl placed by the distance method. The membrane-protein model was immersed in a cubic box of approximately 150 × 150 × 210 Å<sup>3</sup> containing TIP3P waters.

#### 4.3. Molecular dynamics simulation

All-atom simulations of the trimeric complex in the membrane-embedded environment were performed in Gromacs 2021.3 [58]. After an energy minimization step, the equilibration stage consisted of two steps of the NVT (fixed number of particles, volume, and temperature) ensemble followed by four steps of the NPT (fixed number of particles, pressure, and temperature) ensemble to reach 310 K and 1 bar pressure. During the equilibration steps, restraint forces were applied (initially, 4000 kJ/mol/nm on protein backbone; 2000 kJ/mol/nm on protein sidechains; 1000 kJ/mol/nm on lipids; and 1000 kJ/mol/rad<sup>2</sup> on lipidic dihedral angles), which were reduced stepwise to 50, 0, 0 kJ/mol/nm and 0 kJ/mol/rad<sup>2</sup>, respectively. The production phase consisted of 500 ns of unrestrained simulation.

Using the same protocol, an MD simulation of FtsQ inserted into the membrane was also carried out, starting from its AlphaFold 2 model.

#### 4.4. Structural analyses

VMD [59] was used for the visualization of simulation results. In each trajectory, a cluster analysis was performed with Gromacs using the gromos method [60]. The clustering was based on the root-mean-square deviations (RMSD) of Cα atoms with cutoff values of 0.4 nm for the FtsQBL complex and 0.45 nm for free FtsQ. The central structure of the largest cluster was used as the most representative structure for analysis. For the trimeric complex, the most representative FtsQ model (FtsQ in FtsQBL, ‘complexed state’) was also obtained separately. Global structural variations were determined on Cα atoms with MDLovoFit [61]. From this, a threshold was set at having 70% of residues representing the fixed core of the protein or complex, using a reduced trajectory containing 1000 frames at 0.5 ns intervals. The RMSD of the trajectory was calculated with reference to the respective most representative structure. The root-mean-square-fluctuation (RMSF) of residues was calculated with Cα atoms for the whole complex, as well as for the individual FtsQ within the complex. The tilting angle of transmembrane helices was calculated with Gromacs (gmxbundle), with reference to the Z-axis, which is normal to the membrane planes. The vertical distance of the CCD

from the membrane surface was calculated with Gromacs (gmxdistance) as the Z-component of the separation between the center of geometry of each group of CDD Cα atoms (FtsB residues 55–59 and FtsL residues 88–94), with reference to the center of geometry of three manually-selected widely separated phosphorus atoms on the membrane upper leaf.

Bio3D [62,63], an R library package, was employed for principal component analysis (PCA), dynamic cross-correlation matrix (DCCM) and difference distance matrix (DDM) calculations and correlation network analysis (CNA). These analyses employed Cα-atoms only which informed on the protein backbones. DCCM was calculated with Cα atoms with no filters and values normalized to be between −1 (anti-correlated) and 1 (fully correlated).

#### 4.5. Difference distance matrix

A residual difference distance matrix (DDM) of FtsQ was constructed from the pair of trajectories using the Bio3D eDDM module. Long-range interactions were excluded by applying a contact-maps mask. The maps were constructed from the respective trajectories to allow only Cα–Cα distances > 1 Å and < 8 Å for consideration. Statistically important changes were defined as those having a *p*-value < 0.005 and an absolute distance > 3 Å.

#### 4.6. Contact network analysis

Protein correlation networks were constructed over the MD trajectory, sampling at 0.5 ns intervals (1000 frames). The Girvan-Newman betweenness algorithm was employed for community clustering. The FtsQBL complex was approximated into a coarse-grained contact network from a DCCM of Cα atoms, with a cutoff set to screen out values below 0.3. A contact map was applied to filter out long-range (> 10 Å) and statistically insignificant interactions (contact probability < 0.75). Finally, the network was re-modelled to remove single-residue segments contained in some communities (Xin-Qiu Yao, personal communications).

The structural and dynamical properties of FtsQ in the free and complexed states were subjected to difference contact network analysis (dCNA) [64]. Two residues are considered to be in contact if their heavy atoms were within 4.5 Å and existed for > 75% of the trajectory. The default threshold of 0.9 was used in defining a stable contact and contact frequencies below the threshold of 0.1 were discarded. The consensus communities for analysis were determined from the trajectories of free and complexed FtsQ.

#### CRediT authorship contribution statement

**Yu Wai Chen:** Conceptualization, Methodology, Formal analysis, Investigation, Data curation, Writing – original draft, Visualization, Writing – review & editing, Supervision. **Wai-Po Kong:** Conceptualization, Formal analysis, Investigation, Writing – original draft, Visualization, Writing – review & editing. **Kwok-Yin Wong:**

Conceptualization, Resources, Writing – review & editing, Project administration, Funding acquisition.

## Data Availability

The most representative model of membrane-embedded FtsQBL is available in the ModelArchive (modelarchive.org) with the accession code ma-joat3. The model of FtsQ is also available with the accession code ma-c5gg3. The trajectory files are available upon request from the authors.

## Declaration of Competing Interest

The authors declare that they have no known competing financial interests or personal relationships that could have appeared to influence the work reported in this paper.

## Acknowledgements

We would like to acknowledge Google Colaboratory (Colab) for its freely-accessible computational platform for research. Xin-Qiu Yao and Donald Hamelberg were extremely helpful in offering timely support on the general use of Bio3d, as well as on dCNA and eDDM analyses. Likewise, Leandro Martinez provided immediate support for the MDLovoFit program. Part of this work was performed at the University Research Facility in Big Data Analytics (UBDA), Hong Kong Polytechnic University. KYW acknowledges the support from the Patrick S.C. Poon endowed professorship. This work was funded by the Ministry of Science and Technology of China (P0011953) and the Hong Kong Innovation and Technology Commission.

## Appendix A. Supporting information

Supplementary data associated with this article can be found in the online version at doi:10.1016/j.csbj.2023.03.052.

## References

- [1] Vicente M, Rico AI, Martinez-Arteaga R, Mingorance J. Septum enlightenment: assembly of bacterial division proteins. *J Bacteriol* 2006;188:19–27. <https://doi.org/10.1128/JB.188.1.19-27.2006>
- [2] Du S, Lutkenhaus J. Assembly and activation of the *Escherichia coli* divisome. *Mol Microbiol* 2017;105:177–87. <https://doi.org/10.1111/mmi.13696>
- [3] Cho H, Uehara T, Bernhardt TG.  $\beta$ -lactam antibiotics induce a lethal malfunctioning of the bacterial cell wall synthesis machinery. *Cell* 2014;159:1300–11. <https://doi.org/10.1016/j.cell.2014.11.017>
- [4] den Blaauwen T, Andreu JM, Monasterio O. Bacterial cell division proteins as antibiotic targets. *Bioorg Chem* 2014;55:27–38. <https://doi.org/10.1016/j.bioorg.2014.03.007>
- [5] de Boer PA. Advances in understanding *E. coli* cell fission. *Curr Opin Microbiol* 2010;13:730–7. <https://doi.org/10.1016/j.mib.2010.09.015>
- [6] Rowlett VW, Margolin W. The bacterial divisome: ready for its close-up. *Philos Trans R Soc Lond B Biol Sci* 2015;370. <https://doi.org/10.1098/rstb.2015.0028>
- [7] Trip EN, Scheffers DJ. A 1 MDa protein complex containing critical components of the *Escherichia coli* divisome. *Sci Rep* 2015;5:18190. <https://doi.org/10.1038/srep18190>
- [8] Goehring NW, Gonzalez MD, Beckwith J. Premature targeting of cell division proteins to midcell reveals hierarchies of protein interactions involved in divisome assembly. *Mol Microbiol* 2006;61:33–45. <https://doi.org/10.1111/j.1365-2958.2006.05206.x>
- [9] Haeusser DP, Margolin W. Splitsville: structural and functional insights into the dynamic bacterial Z ring. *Nat Rev Microbiol* 2016;14:305–19. <https://doi.org/10.1038/nrmicro.2016.26>
- [10] Loose M, Mitchison TJ. The bacterial cell division proteins FtsA and FtsZ self-organize into dynamic cytoskeletal patterns. *Nat Cell Biol* 2014;16:38–46. <https://doi.org/10.1038/ncb2885>
- [11] Mosyak L, Zhang Y, Glasfeld E, Haney S, Stahl M, et al. The bacterial cell-division protein ZipA and its interaction with an FtsZ fragment revealed by X-ray crystallography. *EMBO J* 2000;19:3179–91. <https://doi.org/10.1093/emboj/19.13.3179>
- [12] Du S, Pichoff S, Lutkenhaus J. FtsEX acts on FtsA to regulate divisome assembly and activity. *Proc Natl Acad Sci USA* 2016;113:E5052–61. <https://doi.org/10.1073/pnas.1606656113>
- [13] Berezuk AM, Goodyear M, Khursigara CM. Site-directed fluorescence labeling reveals a revised N-terminal membrane topology and functional periplasmic residues in the *Escherichia coli* cell division protein FtsK. *J Biol Chem* 2014;289:23287–301. <https://doi.org/10.1074/jbc.M114.569624>
- [14] Tsang MJ, Bernhardt TG. A role for the FtsQLB complex in cytokinetic ring activation revealed by an ftsL allele that accelerates division. *Mol Microbiol* 2015;95:925–44. <https://doi.org/10.1111/mmi.12905>
- [15] Mohammadi T, van Dam V, Sijbrandi R, Vernet T, Zapun A, et al. Identification of FtsW as a transporter of lipid-linked cell wall precursors across the membrane. *EMBO J* 2011;30:1425–32. <https://doi.org/10.1038/emboj.2011.61>
- [16] Sauvage E, Derouaux A, Fraipont C, Joris M, Herman R, et al. Crystal structure of penicillin-binding protein 3 (PBP3) from *Escherichia coli*. *PLoS One* 2014;9:e98042. <https://doi.org/10.1371/journal.pone.0098042>
- [17] Weiss DS. Last but not least: new insights into how FtsN triggers constriction during *Escherichia coli* cell division. *Mol Microbiol* 2015;95:903–9. <https://doi.org/10.1111/mmi.12925>
- [18] van den Ent F, Vinkenvleugel TM, Ind A, West P, Veprintsev D, et al. Structural and mutational analysis of the cell division protein FtsQ. *Mol Microbiol* 2008;68:110–23. <https://doi.org/10.1111/j.1365-2958.2008.06141.x>
- [19] D'Ulisse V, Fagioli M, Ghelardini P, Paolozzi L. Three functional subdomains of the *Escherichia coli* FtsQ protein are involved in its interaction with the other division proteins. *Microbiol (Read)* 2007;153:124–38. <https://doi.org/10.1099/mic.0.2006/000265-0>
- [20] Gonzalez MD, Beckwith J. Divisome under construction: distinct domains of the small membrane protein FtsB are necessary for interaction with multiple cell division proteins. *J Bacteriol* 2009;191:2815–25. <https://doi.org/10.1128/JB.01597-08>
- [21] Robichon C, Karimova G, Beckwith J, Ladant D. Role of leucine zipper motifs in association of the *Escherichia coli* cell division proteins FtsL and FtsB. *J Bacteriol* 2011;193:4988–92. <https://doi.org/10.1128/JB.00324-11>
- [22] LaPointe LM, Taylor KC, Subramaniam S, Khadria A, Rayment I, et al. Structural organization of FtsB, a transmembrane protein of the bacterial divisome. *Biochemistry* 2013;52:2574–85. <https://doi.org/10.1021/bi400222r>
- [23] van den Berg van Saparoea HB, Glas M, Vernooij JG, Bitter W, den Blaauwen T, et al. Fine-mapping the contact sites of the *Escherichia coli* cell division proteins FtsB and FtsL on the FtsQ protein. *J Biol Chem* 2013;288:24340–50. <https://doi.org/10.1074/jbc.M113.485888>
- [24] Glas M, van den Berg van Saparoea HB, McLaughlin SH, Roseboom W, Liu F, et al. The soluble periplasmic domains of *Escherichia coli* cell division proteins FtsQ/FtsB/FtsL form a trimeric complex with submicromolar affinity. *J Biol Chem* 2015;290:21498–509. <https://doi.org/10.1074/jbc.M115.654756>
- [25] Villanelo F, Ordenes A, Brunet J, Lagos R, Monasterio O. A model for the *Escherichia coli* FtsB/FtsL/FtsQ cell division complex. *BMC Struct Biol* 2011;11:28. <https://doi.org/10.1186/1472-6807-11-28>
- [26] Buddelmeijer N, Beckwith J. A complex of the *Escherichia coli* cell division proteins FtsL, FtsB and FtsQ forms independently of its localization to the septal region. *Mol Microbiol* 2004;52:1315–27. <https://doi.org/10.1111/j.1365-2958.2004.04044.x>
- [27] Liu B, Persons L, Lee L, de Boer PA. Roles for both FtsA and the FtsBLQ sub-complex in FtsN-stimulated cell constriction in *Escherichia coli*. *Mol Microbiol* 2015;95:945–70. <https://doi.org/10.1111/mmi.12906>
- [28] Park KT, Du S, Lutkenhaus J. Essential role for FtsL in activation of septal peptidoglycan synthesis. *mBio* 2020;11. <https://doi.org/10.1128/mBio.03012-20>
- [29] Kong WP, Gong F, So PK, Chen YW, Chan PH, et al. The structural dynamics of full-length divisome transmembrane proteins FtsQ, FtsB, and FtsL in FtsQBL complex formation. *J Biol Chem* 2022;298:102235. <https://doi.org/10.1016/j.jbc.2022.102235>
- [30] Kshammer L, van den Ent F, Jeffery M, Jean NL, Hale VL, et al. Divisome core complex in bacterial cell division revealed by cryo-EM. *bioRxiv* 2022. <https://doi.org/10.1101/2022.11.21.517367>
- [31] Madeira F, Pearce M, Tivey ARN, Basutkar P, Lee J, et al. Search and sequence analysis tools services from EMBL-EBI in 2022. *Nucleic Acids Res* 2022;50:W276–9. <https://doi.org/10.1093/nar/gkac240>
- [32] Scheffers DJ, Robichon C, Haan GJ, den Blaauwen T, Koningstein G, et al. Contribution of the FtsQ transmembrane segment to localization to the cell division site. *J Bacteriol* 2007;189:7273–80. <https://doi.org/10.1128/JB.00723-07>
- [33] Kureisaite-Ciziene D, Varadajan A, McLaughlin SH, Glas M, Monton Silva A, et al. Structural analysis of the interaction between the bacterial cell division proteins FtsQ and FtsB. *mBio* 2018;9. <https://doi.org/10.1128/mBio.01346-18>
- [34] Choi Y, Kim J, Yoon HJ, Jin KS, Ryu S, et al. Structural insights into the FtsQ/FtsB/FtsL complex, a key component of the divisome. *Sci Rep* 2018;8:18061. <https://doi.org/10.1038/s41598-018-36001-2>
- [35] Pichoff S, Lutkenhaus J. Tethering the Z ring to the membrane through a conserved membrane targeting sequence in FtsA. *Mol Microbiol* 2005;55:1722–34. <https://doi.org/10.1111/j.1365-2958.2005.04522.x>
- [36] Gonzalez MD, Akbay EA, Boyd D, Beckwith J. Multiple interaction domains in FtsL, a protein component of the widely conserved bacterial FtsBLQ cell division complex. *J Bacteriol* 2010;192:2757–68. <https://doi.org/10.1128/JB.01609-09>
- [37] Boes A, Olatunji S, Breukink E, Terrak M. Regulation of the peptidoglycan polymerase activity of PBP1b by antagonist actions of the core divisome proteins FtsBLQ and FtsN. *mBio* 2019;10. <https://doi.org/10.1128/mBio.01912-18>
- [38] Sung MT, Lai YT, Huang CY, Chou LY, Shih HW, et al. Crystal structure of the membrane-bound bifunctional transglycosylase PBP1b from *Escherichia coli*. *Proc Natl Acad Sci USA* 2009;106:8824–9. <https://doi.org/10.1073/pnas.0904030106>

- [39] Condon SGF, Mahbuba DA, Armstrong CR, Diaz-Vazquez G, Craven SJ, et al. The FtsLB subcomplex of the bacterial divisome is a tetramer with an uninterrupted FtsL helix linking the transmembrane and periplasmic regions. *J Biol Chem* 2018;293:1623–41. <https://doi.org/10.1074/jbc.RA117.000426>
- [40] Craven SJ, Condon SGF, Diaz Vazquez G, Cui Q, Senes A. The coiled-coil domain of *Escherichia coli* FtsLB is a structurally detuned element critical for modulating its activation in bacterial cell division. *J Biol Chem* 2022;298:101460. <https://doi.org/10.1016/j.jbc.2021.101460>
- [41] Attaibi M, den Blaauwen T. An updated model of the divisome: regulation of the septal peptidoglycan synthesis machinery by the divisome. *Int J Mol Sci* 2022;23. <https://doi.org/10.3390/ijms23073537>
- [42] Britton BM, Yovanno RA, Costa SF, McCausland J, Lau AY, et al. Conformational changes in the essential *E. coli* septal cell wall synthesis complex suggest an activation mechanism. *bioRxiv* 2022. <https://doi.org/10.1101/2022.11.27.518129>
- [43] Muller MP, Jiang T, Sun C, Lihan M, Pant S, et al. Characterization of lipid-protein interactions and lipid-mediated modulation of membrane protein function through molecular simulation. *Chem Rev* 2019;119:6086–161. <https://doi.org/10.1021/acs.chemrev.8b00608>
- [44] Corey RA, Song W, Duncan AL, Ansell TB, Sansom MSP, et al. Identification and assessment of cardiolipin interactions with *E. coli* inner membrane proteins. *Sci Adv* 2021;7. <https://doi.org/10.1126/sciadv.abh2217>
- [45] Weigle AT, Carr M, Shukla D. Impact of increased membrane realism on conformational sampling of proteins. *J Chem Theory Comput* 2021;17:5342–57. <https://doi.org/10.1021/acs.jctc.1c00276>
- [46] Vasan AK, Haloi N, Ulrich RJ, Metcalf ME, Wen PC, et al. Role of internal loop dynamics in antibiotic permeability of outer membrane porins. *Proc Natl Acad Sci USA* 2022;119. <https://doi.org/10.1073/pnas.2117009119>
- [47] Bond PJ, Faraldo-Gomez JD, Deol SS, Sansom MS. Membrane protein dynamics and detergent interactions within a crystal: a simulation study of OmpA. *Proc Natl Acad Sci USA* 2006;103:9518–23. <https://doi.org/10.1073/pnas.0600398103>
- [48] Mirdita M, Schütze K, Moriwaki Y, Heo L, Ovchinnikov S, et al. ColabFold: making protein folding accessible to all. *Nat Methods* 2022;19:679–82. <https://doi.org/10.1038/s41592-022-01488-1>
- [49] Jumper J, Evans R, Pritzel A, Green T, Figurnov M, et al. Highly accurate protein structure prediction with AlphaFold. *Nature* 2021;596:583–9. <https://doi.org/10.1038/s41586-021-03819-2>
- [50] Šali A, Blundell TL. Comparative protein modelling by satisfaction of spatial restraints. *J Mol Biol* 1993;234:779–815. <https://doi.org/10.1006/jmbi.1993.1626>
- [51] Janson G, Grottesi A, Pietrosanto M, Ausiello G, Guarguaglini G, et al. Revisiting the "satisfaction of spatial restraints" approach of MODELLER for protein homology modeling. *PLoS Comput Biol* 2019;15:e1007219. <https://doi.org/10.1371/journal.pcbi.1007219>
- [52] Rowlett VW, Mallampalli V, Karlstaedt A, Dowhan W, Taegtmeier H, et al. Impact of membrane phospholipid alterations in *Escherichia coli* on cellular function and bacterial stress adaptation. *J Bacteriol* 2017;199. <https://doi.org/10.1128/JB.00849-16>
- [53] Pluhackova K, Horner A. Native-like membrane models of *E. coli* polar lipid extract shed light on the importance of lipid composition complexity. *BMC Biol* 2021;19:4. <https://doi.org/10.1186/s12915-020-00936-8>
- [54] Lugtenberg EJ, Peters R. Distribution of lipids in cytoplasmic and outer membranes of *Escherichia coli* K12. *Biochim Biophys Acta* 1976;441(38–47). [https://doi.org/10.1016/0005-2760\(76\)90279-4](https://doi.org/10.1016/0005-2760(76)90279-4)
- [55] Bogdanov M, Pyrshev K, Yesylevskyy S, Ryabichko S, Boiko V, et al. Phospholipid distribution in the cytoplasmic membrane of Gram-negative bacteria is highly asymmetric, dynamic, and cell shape-dependent. *Sci Adv* 2020;6:eaa6333. <https://doi.org/10.1126/sciadv.aaz6333>
- [56] Lee J, Cheng X, Swails JM, Yeom MS, Eastman PK, et al. CHARMM-GUI input generator for NAMD, GROMACS, AMBER, OpenMM, and CHARMM/OpenMM simulations using the CHARMM36 additive force field. *J Chem Theory Comput* 2016;12:405–13. <https://doi.org/10.1021/acs.jctc.5b00935>
- [57] Huang J, MacKerell Jr. AD. CHARMM36 all-atom additive protein force field: validation based on comparison to NMR data. *J Comput Chem* 2013;34:2135–45. <https://doi.org/10.1002/jcc.23354>
- [58] Abraham MJ, Murtola T, Schulz R, Páll S, Smith JC, et al. GROMACS: High performance molecular simulations through multi-level parallelism from laptops to supercomputers. *SoftwareX* 2015;1–2:19–25. <https://doi.org/10.1016/j.softx.2015.06.001>
- [59] Humphrey W, Dalke A, Schulten K. VMD: visual molecular dynamics. *J Mol Graph* 1996;14:27–8. [https://doi.org/10.1016/0263-7855\(96\)00018-5](https://doi.org/10.1016/0263-7855(96)00018-5)
- [60] Daura X, Gademann K, Jaun B, Seebach D, van Gunsteren WF, et al. Peptide folding: when simulation meets experiment. *Angew Chem Int Ed* 1999;38:236–40. [https://doi.org/10.1002/\(SICI\)1521-3773\(19990115\)38:1/2<236::AID-ANIE236>3.0.CO;2-M](https://doi.org/10.1002/(SICI)1521-3773(19990115)38:1/2<236::AID-ANIE236>3.0.CO;2-M)
- [61] Martínez L. Automatic identification of mobile and rigid substructures in molecular dynamics simulations and fractional structural fluctuation analysis. *PLoS One* 2015;10:e0119264. <https://doi.org/10.1371/journal.pone.0119264>
- [62] Grant BJ, Rodrigues AP, ElSawy KM, McCammon JA, Caves LS. Bio3d: an R package for the comparative analysis of protein structures. *Bioinformatics* 2006;22:2695–6. <https://doi.org/10.1093/bioinformatics/btl461>
- [63] Grant BJ, Skjaerven L, Yao XQ. The Bio3D packages for structural bioinformatics. *Protein Sci* 2021;30:20–30. <https://doi.org/10.1002/pro.3923>
- [64] Yao XQ, Momin M, Hamelberg D. Elucidating allosteric communications in proteins with difference contact network analysis. *J Chem Inf Model* 2018;58:1325–30. <https://doi.org/10.1021/acs.jcim.8b00250>